UNIVERSITY OF BUCHAREST
FACULTY OF CHEMISTRY
DOCTORAL SCHOOL IN CHEMISTRY

PhD THESIS
ABSTRACT

Hydrotreatment of alkenes, alkynes and cycloalkenes on structured catalysts on graphene and mesoporous supports

PhD student:
Rizescu Cristina Adriana

PhD Supervisor:
prof. Vasile I. Pârvulescu

Doctoral committee:
President: Prof. Dr. Camelia BALA
Supervisor: Prof. Dr. Vasile I. PARVULESCU

Official referents:
1. Conf. dr. Niculina-Daniela HĂDADE – Babeș-Bolyai University, Cluj-Napoca.
2. Prof. dr. Dan CAȘCAVAL - Gheorghe Asachi Technical University, Iași
3. Prof. dr. Csaba PAIZS – Babeș-Bolyai University, Cluj-Napoca.

2021

Table of content (corresponding to the PhD thesis)

Chapter 5 – Optimization of Pt/B–Al–SBA–15 catalysts activity for the hydroisomerization reaction

Introduction

Research carried out in this thesis focused several objectives: i) labilization of polycyclic aromatic molecules from heavy petroleum fractions and fragmentation into cycloalkanes with low molecular weight by a Diels – Alder coupling. Thus, anthracene and its substituted derivatives were used as references, and Pt/Al-SBA15 and Pt/Al-MCM-41 as catalysts; ii) investigation of microporous 3D carbon materials as replica of beta (*BEA) and faujasite (FAU) zeolites. The as synthesized were investigated in a series of catalytic hydrotransformations of alkenes, alkynes and cycloalkenes; iii) modification/improvement of the catalytic activity of a reduced graphene oxide (RGO) by modifying it by a plasma treatment with activated hydrogen. This treatment focused a rational control/activation of the defects in the graphene monolayer; the catalytic behavior of the resulting materials was studied in the hydrogenation of alkenes; iv) investigation of the effect of the acidity of a mesoporous SBA-15 support in the hydroisomerization of heptane. The acidity was controled by doping with B and Al, respectively. The catalytic performances of these materials were evaluated in the hydrogenation of alkenes; iv) the hydroisomerization of heptane over SBA-15 dopped with B and Al, respectively.

The thesis is structured in 5 chapters. The first one provides a critical analysis of the already reported data related to the investigated topics and the rest of the 4 chapters discuss the obtained experimental results.

Chapter 1

The demand for primary energy is constantly growing and is estimated at about 34% by 2035, with an average of 1.6% per year. In 2010, the fossil fuels accounted for 81% of primary energy, and their share will fall to 75% in 2035. Coal and natural gas can be used as an energy source with minimal preparation after operation, while oil requires a number of preliminary treatments that depend on the field of use. The distillation of oil results in three fractions: light oil, heavy oil fractions and bitumen. Currently, light (conventional) oil is used as the main source in the petrochemical industry. The decline of this resource has led in the recent decades to an increased interest for the unconventional oil [1]. Also, in the current economic context, the demand for high quality petroleum products such as intermediate distillates (diesel, oil) is increasing, while the demand for heavy products (fuel oil and waste products) is decreasing. Therefore, the focus of refineries is maximizing the yield of light products by valorisation of heavy oil fractions. At the same time, environmental concerns have increased, resulting in increasingly rigorous regulations for different petroleum products [2].

Oil refining is an important industrial process with direct effects on daily and industrial activities. Refined products such as gasoline, diesel, kerosene or fuel oil are basic products that provide road, waterborne and air transport. The modern refinery combines the physical processes of separation (distillation, solvent extraction) with catalytic conversion processes (catalytic reforming, hydrotreating, catalytic hydrocracking, catalytic cracking, alkylation, isomerization). The primary products obtained from oil refining are either light (gasoline, liquefied petroleum gas), intermediate (kerosene, diesel) or heavy (heavy gasoline, waste oils) distillates [3, 4].

Compared to physical processes, catalytic processes are more flexible resulting in high yields of liquid fractions. Choosing the right type of reactor is also important in completing its role in this process [5]. Also, refining technology must avoid the formation of coke, clogging and rapid deactivation of the catalyst as factors that decrease the reaction rate. These technologies must also avoid increasing the viscosity and coking, and facilitate cracking and hydrogen addition processes such as hydrocracking, hydrogenation or hydroisomerization [6].

The hydrogenation processes utilized in the oil processing industry are classified as destructive and non-destructive processes. Destructive processes, such as hydrogenolysis or hydrocracking, are characterized by the cleavage of $C - X$ or $C - C$ bonds and are accompanied by the saturation of the obtained fragments by hydrogen leading to products with low boiling points. These processes require high temperatures and high H_2 pressures. Other reactions such as dehydrogenation, isomerization or cyclization may also occur. The non-destructive processes as simple hydrogenation are used to improve the quality of the feedstock or products and are often called hydrotreating [7].

The catalysts used in the oil processing are bifunctional, showing a cracking and a hydrogenation function. Cracking is provided by an acidic support such as aluminosilicates, while hydrogenation by a metal in a sulphided state (NiMo, NiW, CoMo) or a noble metal catalysts (Pt, Pd) [8]. The ratio between these two functions is taylored to improve both the activity and selectivity. The activity, selectivity, stability and quality of the final product are key factors for measuring the performance of the catalysts in these hydrocracking process [9].

Regarding the support, over the time, different types of materials have been utilized such as γ-Al_2O_3, simple and mixed oxides ($TiO_2 - Al_2O_3$ and $SiO_2 - Al_2O_3$), zeolites, mesoporous silicious materials (MCM–41 and SBA–15) and natural and mineral clays [10].
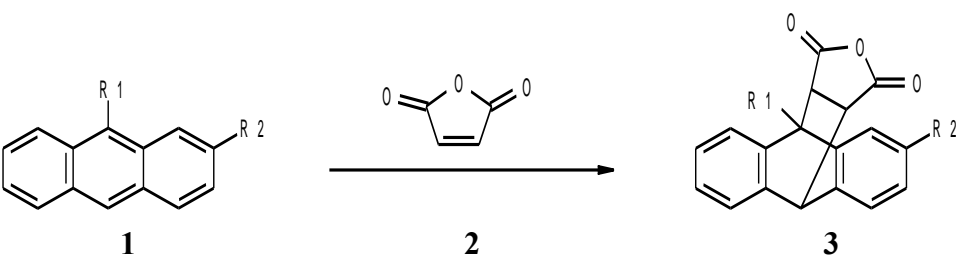
More recently, following sustainable concepts, alternative catalysts such as carbon-based materials have been as well proposed. Thus, carbocatalysis is a developing field aimed to replace the traditional metal-based catalysts [11]. Carbon is known for its various allotropic forms with different properties and structures. Common examples are graphite with sp^2 bonds and diamond

with sp^3 bonds. In recent decades, new nanomaterials composed entirely of sp^2 hybridized carbon atoms have been developed. These include zero–dimensional (0D) fullerenes, one–dimensional (1D) carbon nanotubes and two–dimensional (2D) graphene. Due to their properties, the design and functionalization of the new carbon nanomaterials at the nanoscale level have become a strategy for the synthesis of new materials for various applications. The nanometrically functionalized carbon based materials have specific physical and chemical properties including chemical stability, thermal conductivity, improved mechanical properties, electroconductivity and optical properties that made these prone as catalysts, for environmental science, energy storage, or in biology or medicine [12].

Chapter 2

The research carried out in this chapter started from a new concept, namely, that of destabilization of polycyclic aromatic molecules that are found in heavy oil fractions through a Diels-Alder coupling [13]. Coupling the Diels–Alder reaction with hydrogenolysis aimed at the fragmentation of these molecules into cycloalkanes with low molecular weight. To achieve these objectives, anthracene and its substituted derivatives were used as model molecules and Pt deposited on mesoporous supports of Al–SBA–15 and Al–MCM–41 as catalysts.

Cycloadducts **3** used in this study were obtained with yields between 90 and 93% by the Diels–Alder reaction between several anthracene derivatives **1** and maleic anhydride **2** (Table 1) by modifying a procedure described in the literature [14]. A suspension consisting of anthracene derivative **1** (1 mmol) and maleic anhydride **2** (1.1 mmol) dissolved in 3 mL xylene was refluxed and the evolution of the reaction was monitored by thin layer chromatography (TLC), and at the end, the reaction mixture was cooled. The precipitate obtained was collected by filtration, washed with methanol and dried. The obtained compounds were then recrystallized using a mixture of hexane/ethyl acetate [15].

Table 1. Diels – Alder cycloadducts synthesized in this study

Compound	R_1	R_2	Product	Time (min)	Yield (%)
1a	H	H	3a	30	90
1b	Me	H	3b	30	90
1c	CH=CH$_2$	H	3c	150	93
1d	CHO	H	3d	240	93
1e	H	Et	3e	60	91

The analyzes were performed by TLC (thin layer chromatography) using Fluka silica plates. The structures of the synthesized compounds were confirmed by ^{1}H and ^{13}C NMR spectroscopy. ^{1}H NMR spectra were recorded using a Bruker Avance Ultrashield 500 plus spectrometer at 29 °C and 500 MHz, considering tetramethylsilane (TMS) as the internal standard. ^{13}C NMR spectra were recorded using the same device at 125 MHz. Dimethylsulphoxide (DMSO) having a signal at δ = 39.5 ppm was used as solvent. The compounds were also characterized by IR spectroscopy, the spectra being recorded using a Bruker FTIR Alpha Platinum spectrometer in total attenuated reflectance (ATR).

The catalysts tested in this study were bifunctional mesoporous catalysts, namely Pt–Al–SBA–15 and Pt–Al–MCM–41. The catalytic tests were performed in a 16 mL autoclave purchased from Hell under vigorous stirring (800 rpm) using 0.1 mg Pt(0.5 wt% Pt)–Al–MCM–41 or Pt(0.5 wt% Pt)–Al–SBA–15 and a substrate/Pt molar ratio of 20:1. During the hydrogenation the catalyst was dispersed in 5 mL heptane. The reactions were performed at 100 °C and 30 bar of H$_2$, and the reaction time varied between 1.5–12 h. The reactants and catalyst were charged to the autoclave in an inert atmosphere, and before pressurization the reactor was purged with H$_2$ of three times. The reaction products were analyzed by GC–MS analysis using a Trace GOLD–5SilMS 2000 column coupled with DSQ MS purchased from Thermo Electron Corporation and a GC TRACETM Ultra with Trace GOLD column. The data were purchased and processed using Thermo Scientific Xcalibur software.

The hydrogenation reaction of anthracene took place with high selectivity for the compound dihydroanthracene. In addition to the main product, small amounts of 1,2,3,4,5,6,7,8–

octahydroanthracen and 1,2,3,4,4a,9,9a,10–octahydroanthracen were also obtained. Their hydrogenation continued until perhydroanthracene was obtained, but in traces. This process took place only for Pt–Al–SBA–15. The hydrogenation of **3a–ea** derivatives led to the formation of succinic anhydride and a mixture of hydrogenated derivatives di–, octa– and perhydroanthracene. Dihydroanthracene derivatives were the main products in these hydrogenation reactions. Under the investigated reaction conditions, a total conversion of the cycloadducts was obtained, the degree of hydrogenation depending on the catalyst. Pt–Al–SBA–15 catalyzed a more advanced hydrogenation of aromatic rings than Pt–Al–MCM–41. In the case of derivative **3a**, in addition to perhydroanthracen, tetralin was also obtained, but with a low selectivity (13.3%). For the other derivatives, the hydrogenation stopped with the formation of octahydroanthracene. The exception was the **3e** derivative on the Pt–Al–MCM–41 catalyst, in which case the reaction stopped with dihydroanthracene.

Except for the **3d** derivative, in all other cases the octahydroanthracene derivatives suffered a hydrocracking/decyclization reaction as a result of which tetrahydronaphthalene derivatives were obtained. Decyclization reactions on the Pt/Al$_2$O$_3$ catalyst have been previously reported in the literature [16]. Unlike Pt/Al$_2$O$_3$, on the Pt–Al–SBA–15 catalyst the hydrocracking/decyclization reaction also takes place, even if to a small extent.

Elemental analysis of the tested catalysts indicated a carbon content of less than 1%. The time evolution of the conversion and selectivity confirmed that the 9,10–dihydroanthracene derivative is the first intermediate of the hydrogenation reaction. In the case of compounds **3a–c**, hydrogenation led to the formation of succinic anhydride as a by-product.

The mesoporous texture of the catalysts allowed the hydrogenation of anthracene and the hydrogenolysis/hydrogenation of the Diels–Alder adducts. Regardless of the degree of hydrogenation, the intermediate Diels–Alder coupling is much more energetically favorable for the hydrogenation of polycyclic aromatic compounds. This is also supported by the catalytic tests performed in this study. The hydrogenation of the condensed aromatic compounds took place through a parallel reaction, both at the central ring and at the external ring. Thus, the coupling of the substrate following a Diels–Alder reaction corresponds to a consecutive process that favors the hydrogenation of the central ring. The Pt–Al–SBA–15 catalyst was superior to Pt–Al–MCM–41. It allowed the hydrogenolysis of the adducts and also the hydrogenation of the resulting aromatic rings.

These results show that the Pt deposition proceeded with a different degree of dispersion and particle size on the two supports. For Al–SBA–15 the Pt particles were larger and had a lower

degree of dispersion than for Al–MCM–41. XPS analysis of the two catalysts confirmed the extensive reduction of Pt to Pt^0. In addition to the hydrogenation of anthracene aromatic rings and fragments resulting from the hydrogenolysis of Diels–Alder adducts, due to the bifunctional nature of the catalysts, they were able to catalyze the direct esterification of the by-product (succinic anhydride) to mono– and diesters. The acidity also favored the cleavage of some of the hydrogenated rings by the hydrocracking/decyclization reaction with the formation of hydronaphthalene derivatives. No other alkyl hydronaphthalene derivatives were identified as reaction products, but C4 fragments were also identified. The results obtained corresponded to the thermodynamic calculations, which indicates that the Diels–Alder coupling leads to more energy–stable adducts, in which the extended aromaticity becomes limited.

The acid function of these catalysts is attributed to Al inserted in the networks of the two SBA–15 and MCM–41supports. Pyridine FTIR spectra indicated that this process generated sufficient strong Lewis acid sites to be detected after the desorption of pyridine at 350 °C.

None of the analyzes performed (chromatographic or spectroscopic) indicated the formation of a residual phase. The catalysts were recycled three times after washing with n–hexane and no change in performance was observed. This behavior may be associated with the absence of the repolymerization reaction.

Chapter 3

Chapter 3 dicusses 3D microporous carbon materials synthesized using beta zeolites (*BEA) and faujasite (FAU) as templates. These materials were named β–carbon and Y–carbon, respectively. Their evaluation was performed by comparison with the structure and catalytic properties of conventional graphene and multilayer graphene materials. Their structural and textural properties were investigated using XRD, SEM, TEM and N_2 adsorption, and the coordination of carbon atoms, the presence of defective sites and functional groups were analyzed by complementary spectroscopic methods: XPS, ^{13}C NMR and Raman. Their thermal stability was determined using thermogravimetric analysis (TGA) coupled with differential scanning calorimetry (DSC). The functionality of β–carbon and Y–carbon materials has been demonstrated in a series of catalytic hydrotransformations of alkenes, alkynes and cycloalkenes.

Beta zeolites (* BEA), (NH_4^+ from Si/Al = 11.3, Zeolyst Int., CP814B-25, Lot. No. 814B-25-1597-77) and faujasite (FAU), (H^+ from Si/Al = 6, Zeolyst Int., CBV712, Lot No. 712014001708) were used as templates for the synthesis of 3D graphene type microporous materials named β–carbon and Y–carbon, respectively. The carbonization of zeolites was performed using chemical vapor

deposition with propylene as the carbon precursor, followed by dissolution of the zeolite structure with HF and HCl. Graphene was prepared by pyrolysis of alginic acid at 900 °C in Ar atmosphere and subsequently exfoliated [17], and graphene oxide was prepared by Hummers oxidation of graphite with subsequent exfoliation [18]. These materials have been used as standards for the evaluation of structural and catalytic properties.

The catalytic tests were performed in a 16 mL autoclave reactor purchased from Hell under stirring conditions (800 rpm) using 10 mg of catalyst and 3 mL of substrate pre–treated in an atmosphere of H_2 (5% H_2 in He, 10 mL/min, at 350 °C for 1 h) to remove residual functional groups. The reactions were performed at a pressure of 30 bar of H_2 using heptane as solvent and different reaction times between 1.5–4 h. Prior to pressurization, the autoclave was purged several times with H_2.

The reactants and reaction products were analyzed using a GC–MS chromatograph (Thermo Electron Trace GC Ultra/Trace DSQ) equipped with a non–polar separation column (TG-5SilMS, 30 mx 0.25 mm x 0.25 um) with He as carrier gas. The temperature profile was set to 2 min dwell at 60 °C, 5 °C min^{-1} ramp up to 170 °C, followed by a 5 min dwell. Mass spectra were recorded for positive polarization mode in the range m/z = 50–300. ^1H NMR, ^{13}C NMR, COZY, HMBC and HMQC spectra were recorded in $DCCl_3$ solutions using a Bruker Advance III 500 MHz spectrometer.

The catalytic behavior of β–carbon and Y–carbon materials was evaluated in the transformation of a series of alkenes (1-hexene, 1-octene, 1-decene), cycloalkenes (cyclohexene) and alkynes (1-hexine, 1-phenyl-1-hexine) in the hydrogenation reaction. The ability of 3D graphene like materials to catalyze the hydrogenation of double or triple bonds in linear or cyclic molecules was investigated using 1-hexene, 1-hexine and cyclohexene as model molecules.

1-Hexene was selectively hydrogenated to hexane, without oligomerization or isomerisation products. Hydrogenation of 1-hexine followed the same path resulting in the formation of 1-hexene and hexane, 1-hexene being the main product. The hydrogenation of cyclohexene led selectively to cyclohexane with a reaction rate four times faster than the hydrogenation rate of the linear compounds 1-hexene or 1-hexine. These results indicate that the curved surface of the β– carbon and Y– carbon layers with a high unsaturation degree activates the hydrogen and the substrate molecules promoting the hydrogenation of multiple C–C bonds in the absence of active metal sites. Comparative data for hydrogenation of multiple C–C bonds in linear molecules and significantly increased conversion in the cyclic molecule indicate the important role of substrate structure (electronic and steric effects) as well as the chemosorption mode of the reactant molecule which may affect the insertion of hydrogen.

Previous studies using conventional graphene have shown that monolayer graphene allows the activation of hydrogen and hydrocarbons for the catalytic hydrogenation of multiple C–C bonds in the case of unsaturated hydrocarbons [17]. Hydrogen adsorption energy on metal clusters is up to an order of magnitude larger, and the hydrogen adsorption surface on 3D carbon is three orders of magnitude larger than on a metal catalyst [19]. However, the activation of hydrogen on a flawless graphene basal plane is known to be prevented by the unfavorable energy blocking of the surrounding carbon atoms induced by the sp^3 type bonding of an isolated hydrogen atom. This barrier is not present in β–carbon and Y–carbon materials, în which the centers of the sp^2 surface are accessible to hydrogen and, in addition, the interaction with hydrogen becomes favored by the curvature of the sp^2 surface suitable for these bonds [20]. The reciprocal surface curvature for 3D carbon materials and the presence of a population of unsaturated sp^2 carbon atoms on the edges of the layer are favorable factors that diminish the barrier of activating the interaction between hydrogen and the carbon surface [21]. The activity of β–carbon in hydrogenation reactions is significantly higher compared to that of Y–carbon, having a similar specific surface area, indicating that it is controlled by other factors, such as the number or nature of active sites and/or local structure with a certain curvature of the graphene layer. Creation of individual active sites in metal free graphene for heterogeneously catalyzed acido–basic, oxidation and hydrogenation reactions, has been associated in the literature with the presence of oxygen functional groups, carbon defects or vacancies [17]. The role of unsaturated centers on graphene sheets and the curvature of the layers are especially important to facilitate hydrogenation reactions, as recently shown by Primo et al. [22]. Removal of carbon atoms from graphene layers and the extremities of these surfaces generates monovacancies that induce a metastable structure and can act as active sites for activating hydrogen and substrate chemosorption [20,22]. Therefore, H_2–TPD experiments performed for both 3D graphene like microporous materials can confirm the different concentrations of these carbon centers. For comparison, a monolayer graphene and a defective graphene derived from alginate pyrolysis at 1000 °C indicated as active catalysts for hydrogenation of multiple C–C bonds were analyzed [17]. Graphene generally contains a residual percentage of O that was determined by chemical analysis, as well as carbon vacancies generated by the evolution of CO_2 during the pyrolytic treatment of the graphene structure. The residual percentage of O can be correlated with the acidity of the investigated materials determined from NH_3–TPD experiments , this being similar for all three materials (∼ 0.02 $mmol_{NH3}/g$).

The obtained results showed that β–carbon and Y–carbon showed hydrogen desorption starting from 100 °C. For β–carbon the amount of desorbed hydrogen was 1.6 times higher than for Y–carbon (0.11 and 0.18 $mmol_{H2}/g$ for Y–carbon and β–carbon respectively). The comparison with defective graphene (0.16 $mmol_{H2}/g$) indicates a similar population of defective sites in the structure

of the new β–carbon and Y–carbon materials. The interaction between atomic hydrogen and 3D graphene like materials investigated by Kayanuma et al. showed that hydrogen is predominantly adsorbed on the edge sites of the convex surfaces [23]. The stronger adsorption of hydrogen obtained for β–carbon involves a larger population of defective sites (carbon edges, vacancies and holes). This is consistent with the slightly widened Raman D line width and signal intensity at 30–45 ppm in the ^{13}C CP/MAS and ^{13}C VF/MAS NMR spectra of β–carbon. The larger population of the edge sites is also consistent with a higher proportion of defective pores (mesopore volume 0.08 and 0.5 cm^3/g for Y–carbon and β– carbon, respectively) dominant in the case of less faithfully replicated channels of β–zeolite. The high density of these active sites is β–carbon compared to Y–carbon facilitates high conversions in hydrogenation reactions, as can be seen for the hydrogenation of alkenes, cycloalkenes and alkynes. Other parameters such as specific carbon edge structures, vacancies, holes and curved sheet may also contribute to a different activity.

The reactions with 1-octene and 1-decade were much more interesting. The formation of the corresponding n-alkane was accompanied by intramolecular rearrangements including relocation of the double bond and branching of the linear chain. Skeletal isomerism in both cases led to the selective production of 2-methyl-1-alkene without the formation of other branched molecules. The isomerization of the double bond led to the selective obtaining of the linear alkenes 2-ene (for 1-octene and 1-decene) and 4-ene (for 1-decene). These reactions clearly demonstrate the bifunctional properties of the investigated materials as acid hydrogenation catalysts. In order to be able to confirm the mechanism of double bond and skeletal isomerization by forming an intermediate on an acid site, other experiments were performed in which methanol was added over 1-octene to block the potential acidic sites of the catalysts. Indeed, the addition of methanol increased the selectivity for n-octane with a corresponding decrease in the selectivity for 2-methyl-1-heptene.

Based on these results, it has been concluded that these materials promote two competing mechanisms, one involving the reduction of alkene and the second involving the participation of acidic functional groups present on graphene for the isomerization reaction (Scheme 1).
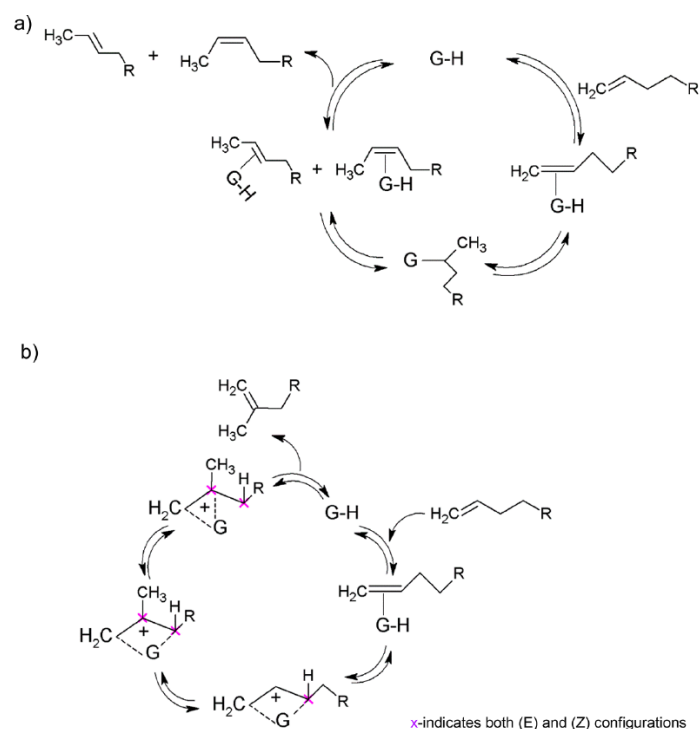
Scheme 1. a) Double bond Isomerization and b) Skeletal isomerization of 1-alkenes on β–carbon and Y–carbon

Hydrogenation of 1-phenyl-1-hexine was performed to support the unique effect of β–carbon and Y–carbon materials on stereocontrol in a catalytic reaction. For this reaction, the difference between the diastereoisomers (E)-1-phenyl-1-hexene and (Z)-1-phenyl-1-hexene was highlighted. While the conversion was slightly higher for β–carbon, the E/Z ratio was about 5 for both materials, indicating that the main product, the E isomer, is more thermodynamically stable.

The stability of β–carbon and Y–carbon catalysts was verified by recycling the catalysts four times. For the hydrogenation reaction of 1-octene the tests did not indicate any loss of activity or selectivity. Also no polymerization of the alkene was observed. Additional experiments were performed by successive hydrogenation of 1-octene and, after cleaning the surface in hydrogen flow, of 1-hexine. The tests confirmed the reproducibility by the conversion and selectivity values.

To highlight the catalytic properties of 3D graphene like materials, the activity of β–carbon and Y–carbon catalysts was compared with that of graphene and graphene oxide. This comparison was performed in the hydrogenation reaction of 1-octene using the same conditions. In addition, the activity of conventional graphite and activated carbon was evaluated. The tests performed using graphite and activated carbon in this hydrogenation reaction indicated a much more modest performance than the graphene catalyst, thus underlining the importance of the electronic structure of these materials [24].

The comparison of the activity of graphene and graphene oxide with the activity of β–carbon and Y–carbon catalysts shows important differences. Thus, graphene oxide showed very low activity, while graphene activity was only slightly higher than that of Y–carbon. In contrast, β–carbon showed superior activity.

The very low activity of graphene oxide in the hydrogenation of the C–C double bond has been highlighted by previous studies [17,24], reconfirming that functional groups with oxygen cannot act as active sites in hydrogenation reactions. In addition, the absence of branched products indicates that a complex interaction between the present oxygen groups and the surface sites in the case of reduced graphene is required to activate the acid catalyzed reactions. The high population of defective sites (edges, vacancies and holes) highlighted by H_2–TPD, Raman and ^{13}C CP/MAS and ^{13}C VF/MAS NMR experiments, in correlation with the curved complex surface of β–carbon induce catalytic activity for hydrogenation. This activity is superior to that presented by the graphene. Another significant advantage of 3D graphene like materials is the relatively simple synthesis that can be achieved on a large scale using cheap zeolites. Their application in a reproducible catalytic process is favored [25].

Curved monolayer carbon layers of β–carbon and Y–carbon materials were spatially structured leading to stable 3D configurations, similar to the channel system in the ordinary crystalline structure of zeolites but with a surface area comparable to the theoretical one of the graphene. The curved surface of the 3D graphene like structure, with porosity accessible through the channel system and the presence of unsaturated carbon atoms on the edges, together with a low concentration of oxygen functional groups facilitates the hydrogenation of multiple C–C bonds that is accompanied by intramolecular rearrangements for selective relocation of the double bond, skeletal and stereoselective isomerization. The research presented in this chapter has highlighted specific properties of monolayer carbon catalysts. These materials can form a new class of catalysts, characterized by high specific surface area and thermal stability.

The catalytic behavior of β–carbon and Y–carbon materials was evaluated in the transformation of a series of alkenes (1-hexene, 1-octene, 1-decene), cycloalkenes (cyclohexene) and alkynes (1-hexine, 1-phenyl-1-hexine) in the hydrogenation reaction.

Through these reactions, 1-hexene was selectively hydrogenated to hexane, without other oligomerization or isomerisation products. Hydrogenation of 1-hexine followed the same pathway resulting in the formation of 1-hexene and hexane, 1-hexene being the main product. The hydrogenation of cyclohexene led selectively to cyclohexane with a reaction rate four times faster than the hydrogenation rate of the linear 1-hexene or 1-hexine.

The reactions with 1-octene and 1-decene were much more interesting. The formation of the corresponding n-alkane was accompanied by intramolecular rearrangements including relocation of the double bond and branching of the linear chain. Skeletal isomerism in both cases led to the selective production of 2-methyl-1-alkene without the formation of other branched molecules. The isomerization of the double bond led selectively to linear 2-ene (for 1-octene and 1-decene) and 4-ene (for 1-decene).

Hydrogenation of 1-phenyl-1-hexine was performed to support the unique stereocontrol effect of β–carbon and Y–carbon materials.The results highlighted the (E)-1-phenyl-1-hexene and (Z)-1-phenyl-1-hexene diastereoisomers in different ratios.

Chapter 4

The research conducted in this chapter aimed to modify/improve the catalytic activity of reduced graphene oxide (RGO) by modifying it by treatment with activated plasma hydrogen. These treatments aimed to achieve a control/mode of activation of defects in the graphene monolayer, subsequently correlating the degree of its exposure with the catalytic performance in the hydrogenation reaction of alkenes. Another objective of this study was to interpret the results by mechanical-quantum calculations on models that indicate how the vacancies created by an atom (monovacancies) or two carbon atoms (vacancies) interact with molecular hydrogen. The aim of these models was to highlight the mechanism by which hydrogen plasma treatment can generate graphene catalysts with controlled activity. These models aimed to highlight the mechanism by which hydrogen plasma treatment can generate graphene catalysts with controlled activity.

The graphene oxide (RGO) used in these studies was obtained by Hummers–Offeman oxidation of graphite, followed by sonic exfoliation and hydrothermal reduction according to a procedure reported in the literature [26].

Then, the RGO sample was treated in a continuous stream of hydrogen. For this, a cylindrical glass plasma reactor (internal diameter 65 mm) with two planar electrodes (diameter 40 mm) placed on the reactor axis was used. The distance between the electrodes was 45 mm. The reactor chamber was evacuated at a pressure of $3{\times}10^{-3}$ mbar after which it was purged with hydrogen at a continuous flow rate of 5 mL/min. The resulting working pressure was 0.1 mbar. The negative DC voltage was applied to one of the electrodes, while the second electrode was grounded.

The discharged voltage was measured using a Tektronix P6015A voltage probe connected to an oscilloscope. The experiments were performed at discharge voltages in the range of 500–800 V. The

corresponding discharge power was between 0.4 W and 2W. The material was placed in a negative discharge chamber. Plasma treatment time range was from 15 to 60 minutes. Through this methodology, graphene samples were prepared under treatments at different powers. Table 2 shows the conditions for their preparation. The first number in the code corresponds to the discharge power and the second number to the treatment time.

Tabel 2. Samples prepared in the present study and relevant parameters of the plasma treatment			
Sample	Discharge voltage (V)	Discharge power (W)	Treatment time (min)
G0.4/60	500	0.4	60
G1.1/15	660	1.1	15
G1.1/30	660	1.1	30
G1.1/60	660	1.1	60
G2/60	800	2	60

Catalytic tests were performed using both plasma treated and un-treated RGO samples in the presence of hydrogen. For comparison, a commercial Beta zeolite (PQ Industries, with a Si/Al molar ratio = 18) and physical mixtures of RGO and Beta zeolite were also investigated. These mixtures were prepared by sonicating the RGO/Beta mixture (1:1 ratio) for 30 minutes. Catalytic tests were performed under stirring conditions (800 rpm) in a 16 mL autoclave reactor purchased from Hell using 10 mg of catalyst and 3 mL of substrate (cyclohexene/1-octene). The experiments were performed at 120 °C for cyclohexene and at 80 °C for 1-octene, at a pressure of 30 bar H_2, using heptane (3 mL) as solvent and reaction times between 1.5–4 h. All used compounds were purchased from Sigma–Aldrich. Before pressurizing, the autoclave was purged several times with H_2.

The reactants and reaction products were analyzed using a GC–MS chromatograph (Thermo Electron Trace GC Ultra/Trace DSQ) equipped with a nonpolar separation column (TG-5SilMS, 30 mx 0.25 mm x 0.25 um) using He as carrier gas. The temperature profile was set to 2 min dwell at 60 °C and 5 °C min ramp up to 170 °C, followed by a 5 min dwell. Mass spectra were recorded for positive ions and in full scan mode positive ions in the range m/z = 50–300.

Theoretical calculations were performed using the Gaussian 09 program [27]. The optimization of the geometry was performed using two theoretical models and basic sets. Geometric calculations were initially performed with a PBE0 hybrid functional at 6–31G (d) considering as model a 4×4 graphene layer terminated H atoms. All optimizations considered statistical analyzes to characterize graphene layers in minimum energy transition or metastable state. In addition, the role of spin

multiplicity (from singlet to triplet) on graphene geometry as well as the overall energy of the system was studied. The energies (E_f, in eV) of the vacant positions in graphene have been defined as follows [28]:

$$E_f = E_d + nE_c - E_p$$

where E_d and E_p are the energies of the structures optimized for defective graphene and perfect graphene, respectively. E_c is the energy for the removed carbon atom, while n has the value 1 or 2 depending on the number of removed carbon atoms to create the vacancies. The chemosorption energies (eV and kcal/mol) between the defective graphene and molecular H_2 at PBE0/6–31G (d) were calculated using the relation:

$$\Delta E_{adsorption} = E_{complex} - E_{grafene} - E_{H2}$$

where $E_{complex}$ is the energy corresponding to the graphene defective complex, and $E_{grafene}$ and E_{H2} are the energies optimized for the defective individual graphene and chemosorbed H_2 molecules, respectively.

The positive effect of plasma irradiation on the activity of the hydrogenation catalyst is reflected in the conversions calculated for the liquid phase hydrogenation of cyclohexene over various graphene samples. The results confirm that the treated graphene not only indicate the hydrogenation of cyclohexene to cyclohexane as a single product [29, 30], but change its catalytic activity with the power and duration of plasma exposure treatment. These results show a catalytic order similar to that observed for cyclohexene and for 1-octene too, used as substrate. Additionally, in this case, the distribution of the products includes position and skeletal isomers of 1-octene, as well as octane. The variation in time of the conversions for 1-octene reaction shows that the graphene activity increases with the power and time of exposure to hydrogen plasma. Compared to cyclohexene under similar conditions the conversion of 1-octene is negligible.

The use of 1-octene as a substrate allows a better understanding of the effect of the changes produced on the modified graphene oxide by exposure to hydrogen plasma. Thus, regarding the selectivity of the reaction, the formation of the 2-methyl-1-heptene skeletal isomer is relevant. The variation in the selectivity as a function of time showed that the RGO sample leads mainly to octane and in a small extent, of 2-octene. Modification of graphene functionality by an additional generation of OH functional groups with reduced acidity by plasma irradiation, orients the skeletal isomerization leading to 2-methyl-1-heptene, a compound that is also found in the other catalytic tests. The formation of this product requires a bifunctional catalyst, and therefore, this process is usually observed for noble metal catalysts supported on an acidic solid supports [31,32]. In addition, the selectivity to 2-methyl-1-heptene reaches a maximum of 15.5% for sample G1.1/30.

The total conversion to isomerization products on the G1.1/30 catalyst was about 31%. By correlating with the chemosorption data of H_2, H_2–TPD, XPS and DRIFT spectroscopy, the behavior of the G1.1/30 sample corresponds to an intermediate population of acid groups and an average defect density. This interpretation is consistent with the NH_3–TPD results on the graphene sample. NH_3–TPD measurements showed that the acidity changes with the hydrogen plasma treatment and the most acidic samples are those obtained at low plasma energies and short irradiation times (see samples G1.1/15 and G1.1/30). This acidity decreases as the exposure time or plasma power increases. These results are in agreement with the assumption that skeletal isomerization, which produces 2-methyl-1-heptene, requires a balance of the catalyst between acidity and hydrogenation activity.

To confirm the role of acidity in the skeletal hydroisomerization of 1-octene, additional experiments were performed to evaluate the catalytic behavior of a 1:1 mixture of Beta zeolite and RGO. The results showed a variation of conversion and selectivity at different reaction times for Beta zeolite, RGO and a 1:1 Beta/RGO physical mixture in the 1-octene reaction. In accordance with the high acidity, in the presence of Beta zeolite the conversions in 1-octene hydroisomerization were much higher than RGO graphene.

DFT calculations were performed to justify the role of holes (defects) in the graphene layer on the activity. Theoretical calculations considered models of graphene layers containing mono and di-vacancies. Activation of H_2 on the defective surface of graphene considered these sites. DFT calculations were also performed to determine the number of representative C atoms in the model on the geometry. For this purpose geometry models of 2×2, 4×4 and 8×8 carbon atoms, were considered respectively. The optimizations for flawless graphene have led to similar energyes as for which the simplest graphene layer model was chosen (4×4). This model is characterized by $C(sp^2)$–$C(sp^2)$ bond lengths between 1.41 and 1.43 Å, being shorter near the graphene edge (approximately 1.38 Å). The removal of a carbon atom from these structures generates a monovacancy that leads to a metastable graphene where the carbon vacancy causes a restructuration of the sheet with appearance of a 5 and another 9 membered ring. These results are in agreement with previously reported DFT calculations [33].

In order to induce H_2 activation inside the defects of the monovacancy graphene sheet, the positioning of the H_2 molecule inside the vacancy was considered. It was realized that the distance between the centroid $C(sp^3)$–$C(sp^3)$ and the opposite edge of the vacancy has the value of 2.48 Å (Figure 1), being long enough to accommodate an H_2 molecule with a bond length of 0.74 Å – at model level PBE0 / 6-31G (d) – and an estimated total length of 1.04 Å. Then, system constituted by the model of a monovacancy and a H_2 molecule was allowed to relax to the minimum energy.
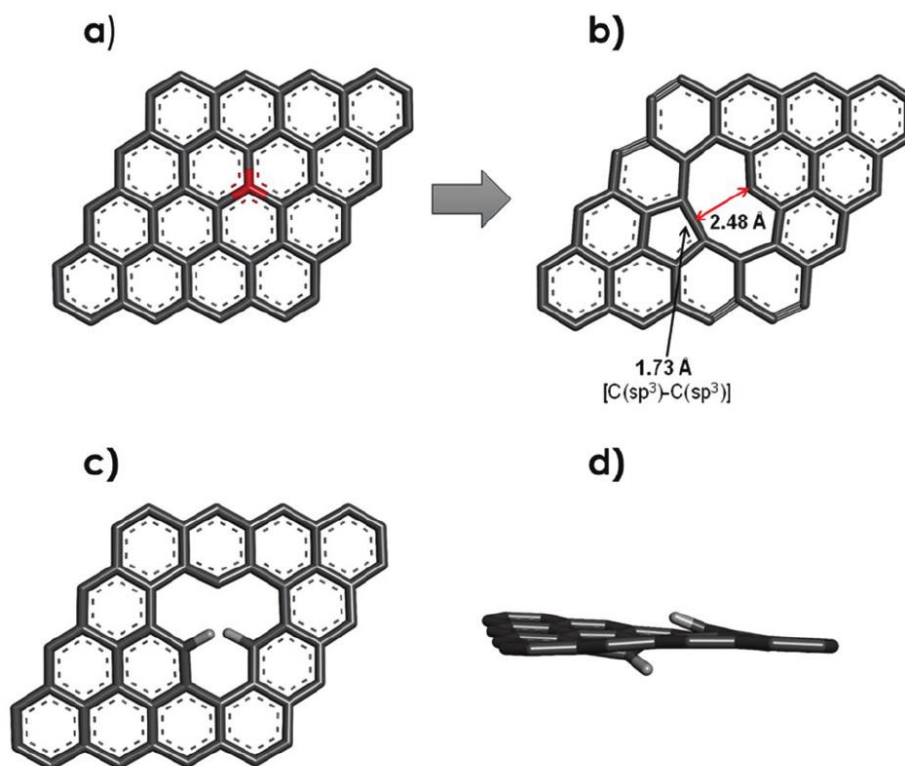
Figure 1. Generation of the carbon vacancy for the 4 × 4 graphene model by removing the carbon atom shown in red in Figure **a**). Generating the resulting model geometry using the PBE0/6-31G protocol (d) **b**). Dissociative adsorption of H_2 on a single vacation presented from two perspectives **c**) and **d**) and calculated by the same protocol. Peripheral hydrogen atoms were omitted.

A different situation results when the 4×4 graphene model considers a hole (Figure 2). Similar to the monovacance model, optimization of the geometry in divacancy models leads to a reconstruction around the defect resulting in the appearance of three new rings of 5, 8 and 5 atoms, respectively. The divergence model retains its flatness after optimizing the geometry with similar average $C(sp^2)$–$C(sp^2)$ bond lengths of approximately 1.43 Å. However, a significant difference was the $C(sp^3)$–$C(sp^3)$ bond lengths which is constrained from 1.73 to 1.56 Å for divacancy model. This behavior is accompanied by an additional stabilization of −0.3 eV as a result of a triplet spin multiplicity compared to the singlet configuration.
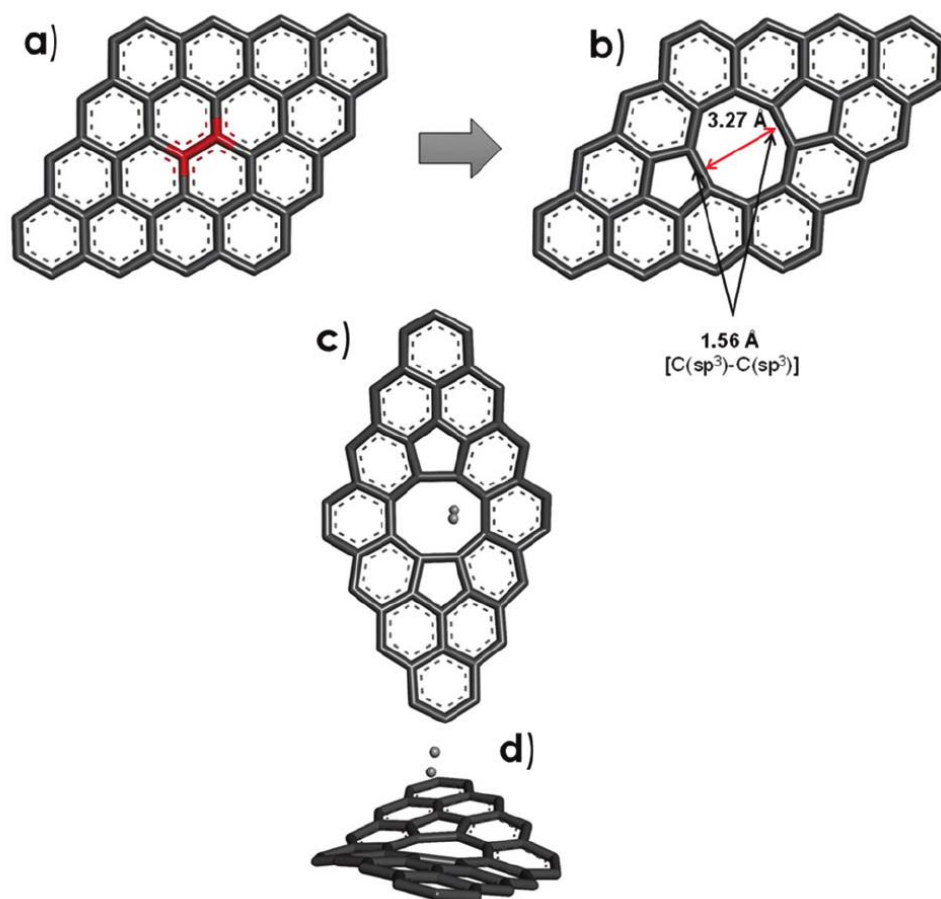
Figure 2. (**a** and **b**) - Formation of divergences in a 4×4 graphene model by removing the atoms indicated in red. The resulting model for divacancy graphene was optimized using the PBE0/6-31G protocol (d). (**c** and **d**) - Top and side view of the H_2 position after optimization considering the same protocol. In all cases the peripheral hydrogen atoms were omitted.

One important feature that arises from the geometry optimization for the double vacancy graphene sheet model is that the distance between the two opposite 5-membered ring edges was 3.27 Å, even larger than that of the graphene model for the monovacancy. This increase in size may play an important role in activating H_2. Recent literature data on Lewis acid-base pairs consider opposite centers at a short distance, proportional to the length of the H_2 bond, but long enough to avoid compensation for acid and base sites [34, 35]. Corroborating with these data, the present study suggests the need for a limited distance for which the H_2 molecule can be activated. These results confirm the need to generate holes with optimal dimensions to produce an efficient activation of H_2.

The outcome of the present calculations with models of graphene sheets for one or two carbon atom vacancies indicated that there is a considerable restructuring of the carbon atoms around the vacancies and that this rearrangement particularly affects the interaction with H_2. Monovacancies appear to interact more strongly with H_2 as a consequence of the better match between distances in the defects generated and the size of the H_2 molecule. This behavior can lead to the formation of C–

H bonds that can block active sites. The determinations performed by DRIFT spectroscopy did not provide any argument in favor of the formation of these C–H bonds. In the case of divacancies, even if their interaction with H_2 molecules is weaker due to the larger size of the defects and the fact that they do not cause an increase in the length of the H_2 bond. Chemosorption on divacancies can have the effect of polarizing H atoms which can lead to some pre-activation of H_2 compared to the hydrogenation of C=C bonds. However, the low adsorption energy and the polarization generated appear to be too weak to cause this activation. Therefore, further evidence is needed regarding the nature of the active sites required for H_2 activation. The involvement of heteroatoms in this process is not excluded. The combination of the DFT calculations and the previously reported H/D isotopic exchange showed that H_2 activation can take place on the vacancies created by carbon atoms, the activation energy depending on how H_2 approaches the active site and the steric hindrance for the allocation of C–H bond [36]. If the acidic properties of a graphene oxide material dominate these materials can catalyze hydrogen transfer reactions [37].

For the catalysts prepared by treating the RGO sample in hydrogen plasma there were generated two types of active sites, a fact confirmed by XPS, DRIFT, chemosorption of H_2 and H_2–TPD. These correspond to a combination of vacancies, which are responsible for hydrogenation reactions, and functional groups such as OH and COOH, which are formed through a disproportionate process and are responsible for the acid behavior. The DFT calculations performed in this study provided theoretical support for these characterization studies. Based on these, the hydrogenation activity can be attributed to the vacancies, while the isomerization is attributed to the acid sites.

The beneficial effect of the hydrogen plasma irradiation on the activity of the catalyst. is also confirmed by the conversion of cyclohexene in the liquid phase hydrogenation. The the plasma treated graphene affords the hydrogenation of cyclohexene to cyclohexane as a single product and modify its catalytic activity with the power and duration of the plasma exposure treatment. The use of 1-octene as a substrate allows a better understanding of the effect of the changes produced on the modified graphene oxide by the exposure to hydrogen plasma. Thus, the formation of the 2-methyl-1-heptene skeletal isomer is relevant in this sense. However, the variation of selectivity as a function of time showed that the RGO leads mainly to octane and to a small extent of 2-octene.

Chapter 5

This chapter aimed to investigate the effect of the acidity of the mesoporous support SBA-15 in the hydroisomerization reaction of heptane. The acidity of the investigated SBA-15 was controlled by dopping with B and Al in Al/Si, B/Si and (Al:0.5–B:0.5)/Si ratios of 1/10. Previous studies have

shown a significant increase in the acidity of Al-SBA-15 compared to the initial support SBA-15 or B-SBA-15 [38].

The supports were synthesized according to a procedure presented in Chapter 2, in which aluminum isopropoxide and/or HBO_3 (M:Si = 1:10) were used as the source of Al and/or B.

Catalytic tests were performed in a 16 mL Teflon-coated autoclave from Hell under stirring conditions (800 rpm), using 10 mg catalyst (0.5% Pt/Al-SBA-15, 0.5% Pt/B-Al-SBA-15 and 0.5% Pt/B-SBA-15) and 4 mL heptane. The reactions were performed at different temperatures (200, 250 and 300 °C), under a pressure of 30 bar H_2 and reaction times in the range of 3–24 h. Before pressurization, the autoclave was purged several times with H_2.

The reaction products were analyzed using a GC–MS chromatograph (Thermo Electron Trace GC Ultra/Trace DSQ) equipped with a non-polar separation column (TG-5SilMS, 30 mx 0.25 mm x 0.25 um) with He as carrier gas. The temperature profile was set to 2 min dwell at 60 °C and 5 °C min ramp up to 170 °C, followed by a 5 min dwell. Mass spectra were recorded for positive ions and in full scan mode in the range m/z = 50–300.

For the investigated time and temperature range, the Al-SBA-15, Al-B-SBA-15 and B-SBA-15 supports did not show catalytic activity for isomerization. Instead, Al-SBA-15 and Al-B-SBA-15 showed activity for cracking, but in a small percentage (less than 5%). This behavior is in line with previous studies regarding the acidic properties of Al-SBA-15 support [39]. However, the deposition of Pt on these supports also afforded the isomerization.

Regardless of temperature or reaction time, the Pt/Al-B-SBA-15 catalyst showed a higher conversion than the Pt/Al-SBA-15 catalyst that well correlate to the acidity of these catalysts [40]. The deposition of Pt on the Al-SBA-15 support was achieved with a larger decrease in the concentration of the strong acid sites compared to Pt/Al-B-SBA-15. The activity of Pt/B-SBA-15 reflects its acidity.

All the investigated Pt/SBA-15 catalysts provided high selectivity for isomerizing compounds, with methyl-hexanes being the main products. Dimethyl-pentanes were also obtained, but in a different extent. As expected, the selectivity for dimethyl-pentanes increased directly proportional to temperature and reaction time. For the Pt/Al-B-SBA-15 and Pt/Al-SBA-15 catalysts, the selectivities for isomers generated maximum values, about 30%, at 300 °C after 24 h, while for the Pt/B-SBA-15 catalyst, the maximum selectivity for dimethyl-pentanes was about 10%. These results are consistent with differences in the acidity of the catalysts.

The isomerization process was accompanied by cracking of heptane to C1–C4 molecules. The activity of the catalysts in this direction was quite weak. For the Pt/Al-SBA-15 and Pt/B-Al-SBA-

15 catalysts, low yields of about 6% for cracking products were obtained, while for the Pt/B-SBA-15 catalyst, the yields were less than 2%.

These reactions were accompanied by the formation of coke. The amount of coke determined from the thermogravimetric analysis of the catalysts after 24 h of reaction was less than 5% of the mass of the catalysts. The addition of B, although it had the effect of an increase in activity, led to an approximately similar coke content (5% for Pt/Al-SBA-15, compared to 4% for Pt/B-Al-SBA-15). The catalyst (Pt/B-SBA-15) with the lowest activity also produced the lowest coke content (less than 1%).

General conclusions

The primary valorisation of oil involves a distillation process that results in three fractions: light oil, heavy oil fractions and bitumen. Of these, light (conventional) oil is used as the main source in the petrochemical industry. However, the decline of this resource has led in recent decades to an interest in capitalizing on the other two factions. In the current economic context, the demand for high quality petroleum products such as intermediate distillates (diesel, oil) is increasing, while the demand for heavy products (fuel oil and waste products) is decreasing. Therefore, maximizing the yield of light products by capitalizing on the heavy fractions of oil is in the momentary attention of refineries.

Given this current state, refining technology must avoid the formation of coke in the process, clogging and rapid deactivation of the catalyst, that is, the factors that have the effect of decreasing the reaction rate. At the same time, these technologies must avoid increasing viscosity and coking, but facilitate cracking and hydrogen addition processes such as hydrocracking, hydrogenation or hydroisomerization.

In view of these considerations, this thesis has set its objectives:

i) destabilization of polycyclic aromatic molecules found in heavy petroleum fractions and fragmentation of these molecules into cycloalkanes with low molecular weight;

ii) deposition of 5% Pt on Al–SBA–15 and Al–MCM–41 to obtain bifunctional catalysts with different dispersions of Pt particles. Pt–Al–SBA–15 contained Pt particles larger than Pt–Al–MCM–41. Both catalysts showed relatively strong Lewis acidity, which was associated with the presence of extra–networked Al species. In order to evaluate these catalysts, in addition to anthracene, a series of adducts were synthesized following the Diels–Alder coupling. The

mesoporous texture of the catalysts allowed the hydrogenation of anthracene and the hydrogenolysis/hydrogenation of the adducts. Consistent with the particle size of Pt, the use of Pt–Al–SBA–15 led to better results for the hydrogenation of anthracene and Diels–Alder adducts. The strong Lewis acidity of the catalysts also allowed the esterification of the secondary reaction product, succinic anhydride, with methanol or ethanol and the fragmentation of the product by hydrocracking/decyclization. The results corresponded to the thermodynamic calculations, which indicates that the Diels–Alder coupling leads to more energy–stable adducts, in which the extended aromaticity becomes limited;

iii) synthesis of microporous 3D carbon materials using beta zeolites (*BEA) and faujasite (FAU) as templates. Curved monolayer carbon layers of β–carbon and Y–carbon materials were spatially structured leading to stable 3D configurations, similar to the channel system in the ordinary crystalline structure of zeolites but with a specific surface comparable to the theoretical specific surface of the graphene. The curved surface of the 3D graphene like structure, with porosity accessible through the channel system and the presence of unsaturated carbon atoms on the edges, together with a low concentration of oxygen functional groups facilitates the hydrogenation of multiple C–C bonds that are accompanied by intramolecular rearrangements for selective relocation of the double bond, skeletal and stereoselective isomerization. The research presented in this chapter has highlighted specific properties of monolayer carbon catalysts. These materials can form a new class of catalysts, characterized by high surface areas and thermal stability. The catalytic behavior of β–carbon and Y–carbon materials was evaluated in the hydrogenation of a series of alkenes (1-hexene, 1-octene, 1-decene), cycloalkenes (cyclohexene) and alkynes (1-hexine, 1-phenyl-1-hexine). Through these reactions, 1-hexene was selectively hydrogenated to hexane, without other oligomerization or isomerisation products. Hydrogenation of 1-hexine followed the same pathway resulting in the formation of 1-hexene and hexane, 1-hexene being the main product. The hydrogenation of cyclohexene took place selectively to cyclohexane with a reaction rate four times faster than the rate of hydrogenation of the linear compounds 1-hexene or 1-hexin. The reactions with 1-octene and 1-decane were accompanied by intramolecular rearrangements including relocation of the double bond and branching of the linear chain. Skeletal isomerism in both cases led selectively to 2-methyl-1-alkene without the formation of other branched molecules. The double bond isomerization took place with the selective production of the linear alkenes: 2-ene for 1-octene and 1-decene and 4-ene for 1-decene. Hydrogenation of 1-phenyl-1-hexine was performed confirmed the unique stereocontrol effect of β–carbon and Y–carbon materials (highlighted by the diastereoisomers (E)-1-phenyl-1-hexene and (Z)-1-phenyl-1-hexene).

iv) control of the modification/ improvement of the catalytic activity of reduced graphene oxide (RGO) by plasma treatment with activated hydrogen with the aim to create a rational activation of defects in the graphene monolayer and enhance the catalytic performance of the resulting materials. With this aim it was investigated the generation of vacancies providing a metal-free catalyst in the hydrogenation reaction. The obtained data were in accordance with a model by which plasma exposure generates defects in the structure of graphene. Hydrogen chemosorption has confirmed an increased capacity of treated graphene and has been correlated with a higher hydrogenation activity. Furthermore, the present O functionality induced a typical activity for bifunctional catalysts (metal/acid) in the hydrogenation reaction of 1-octene. Theoretical calculations considering mono- and divacancy models indicated differences in the H_2 interaction with graphene.

It was also confirmed the possibility of designing active sites by a non-chemical treatment, such as plasma treatment. In addition, hydrogen plasma treatment provided a sustainable way of graphene modification where the maximum energy consumption was of 2 W, which is less than the energy consumed in current thermo-chemical processes. Such a consumption corresponds to a temperature of 3.78 °C for the entire time of the experiments, which is completely insignificant. Under conventional conditions, non-selective chemical changes can only be achieved at temperatures above 500 °C. The effect of these changes was confirmed in the liquid phase hydrogenation of cyclohexene promoted by graphenes exposed to plasma at different powers and times.

Tests with 1-octene allowed a better understanding of the effect of the changes produced in the modified graphene oxide by exposure to hydrogen plasma. Thus, regarding the selectivity of the reaction, the formation of the 2-methyl-1-heptene skeletal isomer is relevant. The variation of the selectivity over time for the hydrogenation of 1-octene in the presence of the graphene showed that the RGO sample mainly led to octane and a small amount of 2-octene. Further, modification of the graphene functionality by additional generation of OH functional groups with reduced acidity by plasma irradiation oriented the skeletal isomerization to 2-methyl-1-heptene. The formation of this product requires a bifunctional catalyst exhibiting an acidic function and a hydrogenation function associated to metal particles.

v) monitoring the effect of the acidity of the mesoporous SBA-15 support in the hydroisomerization reaction of heptane indicated that the partial or total replacement of Al with B had the effect of a slight increase of the surface area, without other obvious effects on the size and volume of the pores. Subsequent deposition of Pt on these supports resulted in a decrease in the surface area, which was more evident for B-SBA-15 and Al-B-SBA-15. This behavior could also be associated with a higher dispersion of Pt particles on the surface of the Al-SBA-15 support, but also with the

effect of acidic conditions during the Pt impregnation process, followed by calcination at 350 ° C for 12 h.

Pt deposition did not damage the support, as demonstrated by both XRD and TEM measurements. The deposition of Pt led, however, to a change in the distribution of acid strength and total acidity of the catalyst, the composition of the support having an important influence in this regard. Al and B exerted a synergistic influence. In this process, the highest concentration of the acid sites was measured for the Pt/Al-B-SBA-15 catalyst which also showed a higher concentration of strong acid sites. The Pt/B-SBA-15 catalyst showed a low concentration of both acidic and strong acidic sites (almost five times). These results demonstrated that Pt anchoring on these supports occurred through the direct interaction of H_2PtCl_6 with the support strong acid sites.

During the investigated time and temperature range, the Al-SBA-15, Al-B-SBA-15 and B-SBA-15 supports did not show catalytic activity for the isomerization. The addition of Pt induced the activity necessary for this reaction even for a weakly acidic support such as B-SBA-15. The Pt/Al-B-SBA-15 catalyst showed the highest conversion. In contrast, the activity of Pt/B-SBA-15 catalyst was twice as low as that of the catalysts containing Al. All Pt/SBA-15 catalysts investigated provided high selectivity for isomerizing compounds, with methyl-hexanes being the main products. Dimethyl-pentanes were also obtained, but in a different extent. The isomerization process was accompanied by cracking of heptane to C1–C4 molecules, but to a rather small extent (yields less than 5% after 24 h).

Originality and perspectives

The originality of the research carried out in this thesis, in line with the proposed objectives, highlighted a number of novelties. The original contributions of the thesis are the following: (i) destabilization of polycyclic aromatic molecules found in heavy petroleum fractions and fragmentation of these molecules into cycloalkanes with low molecular weight by a Diels–Alder coupling. Anthracene and its substituted derivatives were used as sample molecules, and the catalysts tested were Pt/Al-SBA15 and Pt/Al-MCM-41. Their mesoporous texture allowed the hydrogenation of anthracene and the hydrogenolysis/hydrogenation of the adducts. The results obtained corresponded to the thermodynamic calculations which indicated that the Diels–Alder coupling led to more energy–stable adducts, in which the extended aromaticity becomes limited; (ii) synthesis of microporous 3D carbon materials using beta zeolites (*BEA) and faujasite (FAU) as templates. Their assessment was made by comparison with the catalytic structure and properties of conventional graphenes and multi-layer graphenical materials. The synthesized materials, β-carbon

and Y-carbon, were characterized and their functionalities were studied in a series of catalytic hydrotransformations of alkenes, alkynes and cycloalkenes; (iii) modification/improvement of the catalytic activity of reduced graphene oxide (RGO) by modifying by a plasma treatment with activated hydrogen. Through this treatment, a rational control/activation mode of the defects in the graphene monolayer was performed, and the catalytic performance of the resulting materials was studied in the hydrogenation reaction of alkenes. Using this treatment the intention was to create a rational control/activation mode of defects in the graphene monolayer and the catalytic performance of the resulting materials was studied in the hydrogenation reaction of alkenes; (iv) the effect of the acidity of the mesoporous support SBA-15 in the hydroisomerization reaction of heptane. SBA-15 acidity control was performed by doping with B and Al, respectively. Previous studies have shown a significant increase in the acidity of Al-SBA-15 compared to the initial support (SBA-15 or B-SBA-15).

The data obtained in this thesis contain reference elements for future studies such as highlighting and research of the specific properties of monolayer carbon catalysts. These materials represent a new class of catalysts, characterized by specific surface areas and high thermal stability, with very wide applicability in catalysis. Another benchmark that requires further studies is hydrogen plasma treatment as an effective way to produce vacancies in graphene layers. Theoretical calculations considering mono- and divacancy models indicated differences in the H_2 interaction with graphene. For a better understanding and correlation with the experimental results, these calculations still require further rationalization, with the exact structure of the hydrogenation sites still remaining incompletely demonstrated.

Selective Bibliography

[1] A review on the oil-soluble dispersed catalyst for slurry-phase hydrocracking of heavy oil M. T. Nguyen, N. T. Nguyen, J. Cho, C. Park, S. Park, J. Jung, C. W. Lee, Journal of Industrial and Engineering Chemistry 43, (2016) 1–12;

[2] A review of recent advances on process technologies for upgrading of heavy oils and residua M. S. Rana, V. Samano, J. Ancheyta, J. A. I. Dia, Fuel 86, 2007, 1216–1231;

[3] J. Ancheyta, M. S. Rana, Future technology in heavy oil processing, Petroleum Engineering–Downsteam, 2015;

[4] Petroleum refining industry in China W. D. Walls, Energy Policy 38, 2010, 2110–2115;

[5] Hydroprocessing of heavy petroleum feeds: Tutorial J. Ancheyta, M. S. Rana, E. Furimsky, Catalysis Today 109, 2005, 3–15;

[6] In-situ heavy and extra-heavy oil recovery: A review K. Guo , H. Li, Z. Yu, Fuel 185, 2016, 886–902;

[7] J. G. Speight, The Chemistry and Technology of Petroleum, Hydrotreating and Desulfurization, Taylor and Francis Group, New York, 2007, 604–633;

[8] Fischer–Tropsch product as a co-feed for refinery hydrocracking unit P. Šimacek, D. Kubicka, M. Pospišil, V. Rubaš, L. Hora, G. Šebov, Fuel 105, 2013, 432–439;

[9] Hydrocracking of Heavy Oil by Means of In Situ Prepared Ultradispersed Nickel Nanocatalyst S. Alkhaldi, M. M. Husein, Energy Fuels 28, 2014, 643−649;

[10] Hydrocracking of petroleum vacuum residue with activated carbon and metal additives in a supercritical m-xylene solvent T. T. Viet, J. H. Lee, F. Ma, G. R. Kim, I. S. Ahn, C. H. Lee, Fuel 103, 2013, 553–561;

[11] Metal-Free Heterogeneous Catalysis for Sustainable Chemistry D. S. Su, J. Zhang, B. Frank, A. Thomas, X. Wang, J. Paraknowitsch, R. Schlögl, ChemSusChem 3, 2010, 169 –180;

[12] Carbon-based functional nanomaterials: Preparation, properties and applications Z. Li, L. Wang, Y. Li, Y. Feng, W. Feng, Composites Science and Technology 179, 2019, 10–40;

[13] Otto Diels und Wolfgang Ernst Thiele: Zur Kenntnis der Dien-Synthesen, XXX. Mitteil.: Uber das Chlorid der Acetylen-dicarbonsäure O. Diels, W. E. Thiele, Chemische Berichte 71B, 1938, 1173–1178;

[14] Surface chemistry and biological pathogenicity of silicates: an X-ray photoelectron spectroscopic study S. Seal, S. Krezoski, T. L. Barr, D. H. Petering, J. Klinowski, P. H. Evans, Proceedings of the Royal Society of London Series B 263, 1996, 943–951;

[15] Hydrogenation of Condensed Aromatic Compounds over Mesoporous Bifunctional Catalysts Following a Diels–Alder Adduct Pathway P. T. Huyen, M. Krivec, M. Kočevar, I. C. Bucur, C. Rizescu, V. I. Parvulescu, ChemCatChem 8, 2016, 1146 – 1156;

[16] Reaction of Hexane, Cyclohexane, and Methylcyclopentane over Gallium-, Indium-, and Thallium-Promoted Sulfated Zirconia Catalysts V. Pârvulescu, S. Coman, V. I. Parvulescu, P. Grange, G. Poncelet, Journal of Catalysis 180, 1998, 66–84;

[17] Graphenes in the absence of metals as carbocatalysts for selective acetylene hydrogenation and alkene hydrogenation A. Primo, F. Neatu, M. Florea, V. I. Parvulescu, H. Garcia, Nature Communications 5, 2014, 5291–5300;

[18] Graphene oxide as metal-free catalyst for hypochlorite oxidation of primary amines to nitriles A. Primo, M. Puche, O. D. Pavel, B. Cojocaru, A. Tirsoaga, V. I. Parvulescu, H. García, Chemical Communications 52, 2016, 1839–1842;

[19] Chemisorption studies on supported platinum H. L. Gruber, The Journal of Physical Chemistry 66, 1962, 48–54;

[20] Collective stabilization of hydrogen chemisorption on graphenic surfaces D. Stojkovic, P. Zhang, P. E. Lammert, V. H. Crespi, Physical Review B 68, 2003, 195406–195412;

[21] Enhanced Hydrogen Storage Capacity of High Surface Area Zeolite-like Carbon Materials Z. Yang, Y. Xia, R. Mokaya, Journal of the American Chemical Society 129, 2007, 1673–1679;

[22] Graphenes as Metal-free Catalysts with Engineered Active Sites A. Primo, V. I. Parvulescu, H. Garcia, The Journal of Physical Chemistry Letters 8, 2017, 264–278;

[23] Adsorption and diffusion of atomic hydrogen on a curved surface of microporous carbon: A theoretical study M. Kayanuma, U. Nagashima, H. Nishihara, T. Kyotani, H. Ogawa, Chemical Physics Letters 495, 2010, 251–255;

[24] Carbocatalysis: The State of "Metal-Free" Catalysis C. K. Chua, M. Pumera, Chemistry–A European Journal 21, 2015, 12550–12562;

[25] Facile large-scale synthesis of three-dimensional graphene-likeordered microporous carbon via ethylene carbonization in CaX zeolitetemplate K. Kim, Y. Kwon, T. Lee, S.J. Cho, R. Ryoo, Carbon 118, 2017, 517–523.

[26] Preparation of Graphitic Oxide W. S. Hummers, R. E. Offeman, Journal of the American Chemical Society 80(6), 1958, 1339–1339;

[27] M. J. Frisch, G. W. Trucks, H. B. Schlegel, G. E. Scuseria, M. A. Robb, J. R. Cheeseman, G. Scalmani, V. Barone, B. Mennucci, G. A. Petersson, H. Nakatsuji, M. Caricato, X. Li, H. P. Hratchian, A. F. Izmaylov, J. Bloino, G. Zheng, J. L. Sonnenberg, M. Hada, M. Ehara, K. Toyota, R. Fukuda, J. Hasegawa, M. Ishida, T. Nakajima, Y. Honda, O. Kitao, H. Nakai, T. Vreven, J. A. Montgomery Jr., J. E. Peralta, F. Ogliaro, M. Bearpark, J. J. Heyd, E. Brothers, K. N. Kudin, V. N. Staroverov, R. Kobayashi, J. Normand, K. Raghavachari, A. Rendell, J. C. Burant, S. S. Iyengar, J. Tomasi, M. Cossi, N. Rega, J. M. Millam, M. Klene, J. E. Knox, J. B. Cross, V. Bakken, C. Adamo, J. Jaramillo, R. Gomperts, R. E. Stratmann, O. Yazyev, A. J. Austin, R. Cammi, C. Pomelli, J. W.

Ochterski, R. L. Martin, K. Morokuma, V. G. Zakrzewski, G. A. Voth, P. Salvador, J. J. Dannenberg, S. Dapprich, A. D. Daniels, Ö. Farkas, J. B. Foresman, J. V. Ortiz, J. Cioslowski, D. J. Fox, Gaussian 09, Revision D.01, Gaussian, Inc., Wallingford CT, 2009;

[28] Energetics of atomic scale structure changes in graphene S. T. Skowron, I. V. Lebedeva, A. M. Popov, E. Bichoutskaia, Chemical Society Reviews 44, 2015, 3143–3176;

[29] Graphene from Alginate Pyrolysis as a Metal-Free Catalyst for Hydrogenation of Nitro Compounds M. M. Trandafir, M. Florea, F. Neatu, A. Primo, V. I. Parvulescu, H. Garcia, ChemSusChem 9(13), 2016, 1565–1569;

[30] Graphenes in the absence of metals as carbocatalysts for selective acetylene hydrogenation and alkene hydrogenation A. Primo, F. Neatu, M. Florea, V. Parvulescu, H. Garcia, Nature Communications 5, 2014, 5291;

[31] Skeletal Isomerization of Hexane over Pt/H-Beta Zeolites: Is the Classical Mechanism Correct? H. Y. Chu, M. P. Rosynek, J. H. S. Lunsford, Journal of Catalysis 178(1), 1998, 352–362;

[32] Skeletal Isomerization of Hydrocarbons over Zirconium Oxide Promoted by Platinum and Sulfate Ion K. Ebitani, J. Konishi, H. Hattori, Journal of Catalysis 130(1), 1991, 257–267;

[33] Structure and reactivity of carbon multivacancies in graphene M. Oubal, S. Picaud, M. T. Rayez, J. C. Rayez, International Journal of Computational and Theoretical Chemistry 990, 2012, 159–166;

[34] Hydrogen and Amine Activation by a Frustrated Lewis Pair of a Bulky N-Heterocyclic Carbene and $B(C6F 5)3$ P. A. Chase, D. W. Stephan, Angewandte Chemie 47(39), 2008, 7433–7437;

[35] Computational Organic Chemistry: Bridging Theory and Experiment in Establishing the Mechanisms of Chemical Reactions G. J. Cheng, X. H. Zhang, L. W. Chung, L. P. Xu, Y. D. Wu, Journal of the American Chemical Society 137(5), 2015, 1706–1725;

[36] Isotopic H/D exchange on graphenes. A combined experimental and theoretical study G. Sastre, A. Forneli, V. Almasan, V. I. Parvulescu, H. Garcia, Applied Catalysis A 547, 2017, 52–59;

[37] Graphene oxide as a catalyst for the diastereoselective transfer hydrogenation in the synthesis of prostaglandin derivatives S. M. Coman, I. Podolean, M. Tudorache, B. Cojocaru, V. I. Parvulescu, M. Puche, H. Garcia, Chemical Communications 53(74), 2017, 10271–10274.

[38] Direct synthesis of mesoporous M-SBA-15 (M = Al, Fe, B, Cr) and application to 1-hexene oligomerization R. van Grieken, J. M. Escola, J. Moreno, R. Rodríguez, Chemical Engineering Journal 155, 2009, 442–450;

[39] Synthesis and characterization of acidic properties of Al-SBA-15 materials with varying Si/Al ratios G. M. Kumaran, S. Garg, K. Soni, M. Kumar, J. K. Gupta, L. D. Sharma, K. S. Rama Rao, G. Murali Dhar, Microporous Mesoporous Materials 114, 2008, 103–109;

[40] Beta-MCM-41 micro-mesoporous catalysts in the hydroisomerization of n-heptane: Definition of an indexed isomerization factor as a performance descriptor L. Gao, Z. Shi, U. J. Etima, P. Wu, D. Han, W. Xing, S. Mintova, P. Bai, Z. Yan, Microporous Mesoporous Materials 277, 2019, 17–28.

List of publications

Articles:

1. P. T. Huyen, M. Krivec, M. Kojčevar, I. C. Bucur, **C. Rizescu**, V. I. Parvulescu, Hydrogenation of Condensed Aromatic Compounds over Mesoporous Bifunctional Catalysts Following a Diels–Alder Adduct Pathway, ChemCatChem, 2016, 8, 1146 – 1156 (I.F.= 4.803)

2. P. Sazama, J. Pastvova, **C. Rizescu**, A. Tirsoaga, V. I. Parvulescu, H. Garcia, L. Kobera, J. Seidel, J. Rathousky, P. Klein, I. Jirka, J. Moravkova, V. Blechta, Catalytic Properties of 3D Graphene-Like Microporous Carbons Synthesized in a Zeolite Template, ACS Catal., 2018, 8 (3), 1779–1789 (I.F.= 10.614)

3. A. Primo, A. Franconetti, M. Magureanu, N. B. Mandache, C. Bucur, **C. Rizescu**, B. Cojocaru, V. I. Parvulescu, H. Garcia, Engineering active sites on reduced graphene oxide by hydrogen plasma irradiation: Mimicking bifunctional metal/supported catalysts in hydrogenation reactions, Green Chem., 2018, Accepted Manuscript (I.F.= 9.125)

4. **C. Rizescu**, B. Cojocaru, N.T. Thanh Hien, P.T. Huyen, V.I. Parvulescu, Synergistic B-Al interaction in SBA-15 affording an enhanced activity for the hydro-isomerization of heptane over PteBeAl-SBA-15 catalysts, Microporous and Mesoporous Materials 281 (2019) 142–147 (I.F. = 3.64)

5. M. Magureanu, N.B. Mandache, F. Gherendi, **C. Rizescu**, B. Cojocaru, A. Primo, H. Garcia, V.I. Parvulescu, Improvement of catalytic activity of graphene oxide by plasma treatment, Catalysis Today 366 (2021) 2–9 (I.F. = 5.825)

6. M. Magureanu, N.B. Mandache, **C. Rizescu**, C. Bucur, B. Cojocaru, I. C. Man, A. Primo, V. I. Parvulescu, H. Garcia, Engineering hydrogenation active sites on graphene oxide and N-doped graphene by plasma treatment, Applied Catalysis B: Environmental 287 (2021) 119962 (I.F. = 16.683)

Participation in scientific communications:

- **C. Rizescu**, P. T. Huyen, M. Kočevar, V. I. Parvulescu, Diels-Alder coupling facilitating the hydrocracking of heavy fractions, RomCat Conference 2016, The 11th International Symposium of the Romanian Catalysis Society, Timisoara, Romania, 6-8 June 2016

- **C. Rizescu**, P. T. Huyen, V. I. Parvulescu, Hydrogenation of condensed aromatic compounds over mesoporous bifunctional catalysts following a Diels-Alder adduct pathway, EFCATS School on Catalysis, Liblice Castle – June 25-29 2018, Cezh Republic

- P. Sazama, J. Pastvova, **C. Rizescu**, A. Tîrsoaga, V.I. Pârvulescu, H. Garcia, L. Kobera, J. Seidel, J. Rathovsky, P. Klein, I. Jirka, J. Morarkova, Catalytic Properties of 3D Graphene-like Microporous Carbons Synthesized in a Zeolite Template, Pre-symposium of ZMPC2018, "International Symposium on Advanced Zeolite Science & Technology", August 3, 2018, Tokyo, Japan

- **C. Rizescu**, B. Cojocaru, N.T. Thanh Hien, P.T. Huyen, V.I. Parvulescu, Synergistic B-Al interaction in SBA-15 affording an enhanced activity for the hydroisomerization of heptane over Pt-B-Al-SBA-15 catalysts, RomCat Conference 2019, The 12th International Symposium of the Romanian Catalysis Society, Bucharest, Romania, 5-7 June 2019

- A. Primo, A.Franconetti, H. Garcia, M. Magureanu, N. Mandache, C. Bucur, **C. Rizescu**, B. Cojocaru, V.I. Parvulescu, Engineering active sites by hydrogen plasma irradiation: Mimicking bifunctional metal/supported catalysts in hydrogenation reactions, 14th EUROPACAT, Germany, August 18-23, 2019